

# Theoretical Estimates of Intrinsic Galaxy Alignment

Jonathan Mackey<sup>1</sup>, Martin White<sup>1</sup> and Marc Kamionkowski<sup>2</sup>

<sup>1</sup>*Harvard-Smithsonian Center for Astrophysics, 60 Garden St., Cambridge MA 02138*

<sup>2</sup>*Mail Code 130-33, California Institute of Technology, Pasadena, CA 91125*

June, 2001; in final form May, 2002

## ABSTRACT

It has recently been argued that the observed ellipticities of galaxies may be determined at least in part by the primordial tidal gravitational field in which the galaxy formed. Long-range correlations in the tidal field could thus lead to an ellipticity-ellipticity correlation for widely separated galaxies. We present a new model relating ellipticity to angular momentum, which can be calculated in linear theory. We use this model to calculate the angular power spectrum of intrinsic galaxy shape correlations. We show that for low redshift galaxy surveys, our model predicts that intrinsic correlations will dominate correlations induced by weak lensing, in good agreement with previous theoretical work and observations. We find that our model produces ‘*E*-mode’ correlations enhanced by a factor of 3.5 over *B*-modes on small scales, making it harder to disentangle intrinsic correlations from those induced by weak gravitational lensing.

**Key words:** gravitational lensing - cosmology: theory - large-scale structure of Universe

## 1 INTRODUCTION

Galaxy alignments, or ellipticity correlations, have been the subject of much study over many years (Djorgovski (1987), and references therein), extending back well into the 1800s. Once galaxies were discovered and were found to be elliptical in shape, the logical next step was to see if they have a tendency to align with each other. This would provide a clue as to what they were and how they formed. More recently it was realised that different models of structure formation may produce different levels of alignment, and so searches aimed at placing constraints on these models. Searches have historically concentrated in nearby regions of high galaxy density (clusters and superclusters) in order to get good number statistics. The results have been, in general, inconclusive or contradictory of previous results, although weak trends for alignments have been found for some samples (Cabanela & Aldering 1998).

Recently, there has been renewed theoretical interest in long-range correlations of galaxy ellipticities. While initially the interest was in reconstructing the gravitational potential field from the orientations of galaxy spins (Lee & Pen 2000), it has been driven lately by the increasing success of field-surveys for weak gravitational lensing by large scale structure (see Mellier (1999) for a recent review). Weak lensing shear, the coherent distortion of galaxy images on the sky induced by density perturbations along the line of sight (Gunn 1967; Miralda-Escudé 1991; Blandford et al. 1991; Kaiser 1992; Bartelmann & Schneider 1992; Bartelmann & Schneider 1999) has now been detected by several different groups (van Waerbeke et al. 2000; Bacon, Refregier & Ellis 2000; Wittman et al. 2000; Kaiser, Wilson & Luppino 2000; Maoli et al. 2001; Rhodes, Refregier & Groth 2001). Following standard practice, all of these authors assume that all of their observed correlations in the ellipticities of galaxies comes from weak lensing, with an immeasurably small intrinsic signal. Intrinsic correlations, if present, may contaminate the weak lensing signal and so they should be considered when interpreting results from these field-lensing surveys.

Theoretically, alignments are expected at some level because nearby galaxies form in similar and related gravitational fields; they should therefore react in similar ways to the influence of this field and so should have some tendency to align with each other. Several authors have revisited this question recently, with simulations (Heavens et al. 2000; Croft & Metzler 2000) and analytic arguments (Lee & Pen 2000; Catelan, Kamionkowski & Blandford 2000; Crittenden et al. 2001). These authors assume that the ellipticities of the observed luminous galaxies are determined by either the shapes of their dark matter halos or by the halo angular momenta. In either case, the ellipticity should ultimately be determined, at least in part, by the tidal gravitational field in which the galaxy forms. The existence of long-range correlations in the tidal field (Catelan & Porciani 2001) will thus lead to correlations in ellipticities of widely separated sources. Observationally, Pen, Lee & Seljak (2000) report a tentative detection of galaxy alignments in the local universe using the Tully catalog. More recently, Brown et al. (2002) find

a more significant correlation using data from the SuperCOSMOS Sky Survey<sup>\*</sup>. These detections reinforce the importance of considering intrinsic alignments.

An analytic theory of these correlations, even if only approximate, can provide valuable guidance on the plausible shape, size, redshift evolution and sample depth dependence of the effect as well as flag potential indicators of contamination. Catelan et al. (2000) (hereafter referred to as CKB) calculated ellipticity correlations under the assumption that a galaxy’s ellipticity is determined by the initial halo shape. They also outlined an argument for how a galaxy’s angular momentum may determine its ellipticity in the context of the tidal torque theory using the Zel’dovich approximation. A similar model was developed more fully by Crittenden et al. (2001) (hereafter referred to as CNPT) who calculated correlations in ellipticity due to correlations in the direction of the galaxy’s angular momentum vectors. Their model predicts that for low redshift galaxy surveys intrinsic alignments are expected to dominate over weak lensing correlations, with considerable uncertainty in the normalisation. These predictions were later confirmed by the measurements of Brown et al. (2002). In a later paper (Crittenden et al. 2000) they also discuss ways of discriminating between intrinsic correlations and weak lensing induced correlations.

In this paper we build upon some of the ideas presented in CKB, developing an alternate and complementary model to that of CNPT. We calculate in our model how correlations in ellipticity, or “intrinsic shear,” can be generated by correlations in angular momentum, with an emphasis on seeing how large intrinsic correlations can possibly be. While some of the input physics of our model is the same as that of CNPT, our approach and analysis are rather different. CNPT calculate correlations in the direction of the angular momentum only, and for the case where the inertia tensor and tidal field tensor of the protogalaxy are strongly correlated. Our model assumes that these tensors are uncorrelated (numerical simulations have recently produced evidence that this assumption is not justified, see §2.2, although we argue that this assumption does not affect our results significantly), which results in a significantly different expression for the angular momentum generated. It also includes correlations in the magnitude of ellipticities, which may be present. The two models are normalised in different ways, to different physical quantities. In our calculation, we have tried to make approximations that will, if anything, overestimate the ellipticity correlations, in order to place upper limits on their magnitude.

All of these models are really educated guesses as to the relationship between ellipticity and angular momentum, and are also chosen at least partly because of mathematical simplicity. Ideally we would like a quantitative model of galaxy formation which could tell us the relationship between galaxy shape/alignment and the environment in which a galaxy forms. We are currently far from this ideal situation, and so must make certain assumptions for our model which we believe are physically well motivated. It is thus both surprising and gratifying that we obtain very comparable results to CNPT. This may indicate that both our and their conclusions are robust to the considerable simplifications which need to be made in such calculations.

The outline of this paper is as follows. In the next section we discuss our model for relating the angular momentum of a galaxy to its ellipticity in the context of tidal torque theory. In §3 we present our main calculation, explaining in §3.2 how we normalise our model and showing in §3.3 how to relate our results to other measures of correlations. The reader not interested in the details may find the relevant equations summarized in §3.3. We present results for an example ( $\Lambda$ CDM) model in §4, explain them in terms of the underlying physics, and consider the effects of intrinsic correlations on weak lensing measurements of ‘cosmic shear.’ Then in §5, we discuss our results in the context of observations and previous work. We present our conclusions in §6.

## 2 BACKGROUND

In this section we discuss the ingredients of our model. First we introduce the concept and mathematical description of the ellipticity of galaxies. The key assumption we make is that the ellipticity (orientation and magnitude) is determined by the galaxy’s angular momentum. We fix our model so that the ellipticity components transform correctly under rotations in the plane of the sky, and so that the magnitude of the ellipticity of galaxies with more angular momentum is larger. We implicitly assume that the angular momentum of the luminous galaxy is aligned with that of the dark matter halo it resides in. The angular momentum of a galaxy can be predicted and related to the local gravitational potential (in linear theory) using ‘tidal torque theory’. This then allows us to calculate correlations in the ellipticity in terms of correlations in the gravitational potential, which is well specified in linear theory for a given cosmological model.

### 2.1 Galaxy ellipticities

It is a standard assumption in calculations of weak gravitational lensing that the source galaxies are randomly oriented with respect to each other. We wish to investigate to what extent this holds true. Lensing will introduce a shear in the shapes of the sources, so we need to describe any “intrinsic” shear that these sources have, which we do in terms of the spin-2 (complex) ellipticity:

$$\epsilon = |\epsilon|e^{2i\phi} = \gamma_1 + i\gamma_2 . \quad (1)$$

<sup>\*</sup> <http://www-wfau.roe.ac.uk/sss/>

The components  $\gamma_i$  are usually defined in terms of the second moments of the light distribution of a galaxy,  $F(x, y)$ , as

$$\begin{aligned}\gamma_1 &= \frac{\int F(x, y)(x^2 - y^2) dx dy}{\int F(x, y)(x^2 + y^2) dx dy}, \\ \gamma_2 &= \frac{\int F(x, y)(2xy) dx dy}{\int F(x, y)(x^2 + y^2) dx dy}.\end{aligned}\quad (2)$$

It is clear that their values for a given galaxy will depend on the orientation on the sky of the coordinate axes chosen. The correlation functions  $\langle \gamma_i \gamma_j' \rangle$  are obtained by measuring  $\gamma_i$  at one galaxy and  $\gamma_j'$  at another galaxy some distance away on the sky and then multiplying them, doing this for many galaxies separated by the same angular distance, and averaging the result to get the correlation function. Intrinsic shear correlations can be due to correlations in both the magnitude and the orientation of the ellipticity across the sky, both of which are encoded in the components  $(\gamma_1, \gamma_2)$ . For example, if all galaxies were flattened disks with axes of symmetry perfectly parallel with each other, then the correlation would be unity on all scales. If the disks have finite thickness, however, even if galaxies are perfectly aligned, variations in  $|\epsilon|$  with position will cause the correlation to vary with separation. In the opposite limit, if all galaxies are randomly oriented and have random  $|\epsilon|$ , then the correlations are zero and there is no alignment.

We assume that this ellipticity is determined, at least in part, by the galaxy's angular momentum (and hence by the initial tidal field as we show below). For spiral galaxies this is well justified, as the disk angular momentum is perpendicular to the plane of the disk. There is some question as to how closely the angular momentum of the gas and stars in the disk follows that of the dark matter (Abel, Croft & Hernquist, 2001), but it seems reasonable that they should be closely related. Elliptical galaxies tend not to have much net angular momentum, and the ellipticity seems to be determined largely by the velocity dispersion along the principal axes of the 3D ellipsoid. Thus our calculation may be less relevant for elliptical galaxies than for spirals, and the halo shapes calculation of CKB may be more applicable.

Following the angular momentum–ellipticity discussion in CKB, using the assumption that the disk of a galaxy forms perpendicular to the angular momentum, the observed ellipticity of a galaxy will be

$$\begin{aligned}\gamma_1 &= f(L, L_z)(L_x^2 - L_y^2), \\ \gamma_2 &= 2f(L, L_z)L_x L_y,\end{aligned}\quad (3)$$

where we take the sky to be the  $x$ - $y$  plane, and where  $f(L, L_z)$  is an unknown function which determines how ellipticity scales with  $L$ . Since we have no firm theory to predict the form of  $f(L, L_z)$  we will take it to be a constant,  $C$ , whose value must be fitted empirically to the observed rms ellipticity of galaxies. As a result, in our model the ellipticity of a galaxy scales quadratically with its angular momentum, so galaxies with more angular momentum will be more flattened. For the case where galaxies are approximated as thin disks, it can be shown that  $f(L, L_z) = 1/(L^2 + L_z^2)$  (see CNPT), thus taking out the dependence on  $L$ . In this case  $|\epsilon|$  is set to a constant independent of  $L$  and only the orientation is measured by  $\gamma_i$ .

The price we pay for letting  $|\epsilon|$  vary with  $L$  is that galaxies in the tail of the distribution with  $L \gg \langle L \rangle$  can potentially have an unphysical  $|\epsilon| > 1$ . We have calculated the fraction of galaxies this will apply to. In our model ellipticity is proportional to the square of the the gravitational potential (as we show in the next section), and so if we assume the potential fluctuations are gaussian distributed, we can calculate the ellipticity probability distribution from this. The rms ellipticity of galaxies (which we take to be  $\bar{\epsilon} = 0.4$ ; see §3.2) gives the variance of  $|\epsilon|$ . We can thus integrate over the ellipticity probability distribution to find what fraction of galaxies have  $|\epsilon| > 1$ , and we find that this is  $\sim 4\%$ . Larger values of  $|\epsilon|$  are exponentially rare, so they will not affect our calculation in a significant way.

## 2.2 Tidal torque theory

Hoyle (1949) was the first to suggest that galaxies acquire their angular momentum by tidal torques due to the surrounding matter distribution acting on the protogalaxy. This torque comes about from a misalignment of the protogalaxy's mass distribution (inertia tensor) with the local tidal field. Using the Zel'dovich approximation Doroshkevich (1970), and subsequently White (1984), showed that the angular momentum acquired by a protogalaxy to first order in the gravitational potential is

$$L_i(t) \propto \epsilon_{ijk} T_{jl} I_{kl}, \quad (4)$$

where  $T_{ij}$  is the tidal field tensor at the galaxy's centre of mass and  $I_{ij}$  is the inertia tensor of the protogalaxy.

The inertia tensor is given by

$$I_{ij} = \int_{\Gamma} (q_i - \bar{q}_i)(q_j - \bar{q}_j) \rho_0 a^3 d^3 \mathbf{q}, \quad (5)$$

where  $\Gamma$  is the Lagrangian volume of the protogalaxy,  $\mathbf{q}$  is the Lagrangian position vector of the constituent particles with centre of mass  $\bar{\mathbf{q}}$ , and  $\rho_0$  is the background density. We follow CKB in assuming each galaxy has the same eigenframe moment of inertia and the eigenframes are distributed isotropically. Further we suppose that two of the three principle moments are equal, so that the unequal moment defines a symmetry axis  $\hat{\mathbf{n}} = (\cos \theta, \sin \theta \cos \phi, \sin \theta \sin \phi)$ , and so the inertia tensor simplifies to  $I_{ij} \propto n_i n_j$ .

The tidal field tensor is given by

$$T_{ij} \propto \partial_i \partial_j \Phi(\mathbf{x}), \quad (6)$$

where  $\Phi$  is the gravitational potential. All of the proportionality above is time-dependent, but we assume that all our galaxies form at a similar redshift, and so absorb all time dependent quantities into the constant  $C$  above. We normalise our theory in such a way that any time dependence will cancel out.

By inspection of equation (4) it can be seen that if  $\mathbf{I}$  and  $\mathbf{T}$  have the same principal axes then there is no angular momentum acquired to first order. There must be some misalignment between them to generate angular momentum, so the tensors cannot be perfectly correlated. In our calculation we make the simplest assumption, namely that they are completely uncorrelated. Reality lies somewhere in between the extremes of perfectly correlated and uncorrelated. Nevertheless, our expectation is that the large wavelength Fourier modes that are primarily responsible for the long range *correlations* in the tidal field should be statistically independent of the smaller wavelength Fourier modes that are primarily responsible for the inertia tensor. So the hope is that our results should not be very sensitive to this assumption. This assumption comes into play when we calculate the ellipticity correlation function between neighbouring galaxies. We must average over the distribution of inertia tensors and tidal tensors. If the two are uncorrelated we can average over inertia tensors first (as we expect the ellipticity correlation to be due to long range tidal field correlations), and subsequently over the tidal field. Because this assumption is an important part of our calculation, we discuss relevant numerical results in the next section.

## 2.3 Tidal Torque Theory in Numerical Simulations

### 2.3.1 Initial Angular Momentum

Several authors have investigated the questions of angular momentum generation and tidal torque theory (TTT) in numerical simulations. Sugerman, Summers & Kamionkowski (2000) found a relatively good correlation between the predictions of linear theory and the actual evolution of dark matter halos. They found that the Zel'dovich approximation we have used typically overpredicts the magnitude of the angular momentum generated by a factor of  $\sim 3$ , and that the spin direction is marginally reproduced with a large scatter.

Lee & Pen (2000) differed from Sugerman et al. (2000) in that they found quite a strong correlation between the predicted and simulated spin direction, again with a large scatter. They concluded that TTT is a reasonably good predictor of the direction of the angular momentum vector of a halo.

Porciani, Dekel & Hoffman (2002a), in a more detailed study of TTT, used dark matter simulations to look at the spin (i.e. angular momentum) amplitude and direction of halos, as well as spin–spin correlations between halos. They reproduce the result of Sugerman et al. (2000) in finding that TTT systematically overpredicts that amplitude of the spin, but by a constant fraction on average, with a large scatter. The agreement between these two groups is reassuring, and gives us confidence in our calculation. A constant bias in the magnitude of  $\mathbf{L}$  will be taken out by the normalisation of our model, so that the ‘angular momentum’ we calculate really does correspond (on average) to the spin amplitude of a halo.

As regards spin direction, they find that at high redshift, TTT predictions are in good agreement with their simulations, although there is some scatter. They also studied spin–spin correlations of dark matter halos (i.e. correlations in the directions of the spin vectors among neighbouring halos) and find that at high redshift the tidal torque theory reproduces the correlations quite well, albeit with large scatter. These results are important for our calculation in that they show the theory on which it is based to be reasonably accurate, at least at high redshift. The situation is not so good at low redshift, which we return to below.

### 2.3.2 Inertia and Tidal Tensor Correlations

Another important effect is a correlation between the inertia and tidal field tensors. Lee & Pen (2000) found that  $\mathbf{I}$  and  $\mathbf{T}$  were quite strongly correlated in their simulations (although misaligned to a detectable degree), and this conclusion was supported very recently by Porciani, Dekel & Hoffman (2002b). They find that angular momentum is generated by the small but significant misalignment of the tensors. One way of thinking about this is to decompose the inertia tensor into a part perfectly correlated with the tidal tensor, and another part completely random:  $\mathbf{I}_{\text{tot}} = \mathbf{I}_{\text{corr}} + \mathbf{I}_{\text{random}}$  (where we assume for now that different components of  $\mathbf{I}$  and  $\mathbf{T}$  are all correlated at the same level). The correlated part generates no angular momentum to first order so the angular momentum generated is just some fraction of what would have been generated if  $\mathbf{I}$  was all random. The direction is unchanged, only the magnitude is suppressed. Such a situation does not affect our result, because the overall normalization of  $\mathbf{L}$  factors out, as we show in §3.2. Catelan & Theuns (1996) also argued analytically that assuming  $\mathbf{I}$  and  $\mathbf{T}$  are uncorrelated will result in an over-prediction of the magnitude of the angular momentum generated, and this has been verified in simulations (Sugerman, Summers & Kamionkowski 2000; Porciani, Dekel & Hoffman 2002a).

We would see an effect due to  $\mathbf{I}$ – $\mathbf{T}$  correlation if the direction of  $\mathbf{L}$  changed when these two tensors are more strongly correlated. One way to make this happen is if higher order terms become important when this leading order term given by equation (4) is suppressed. Another way is if different components of  $\mathbf{I}$  are correlated with differing strengths to different components of  $\mathbf{T}$ . Such a situation could arise if the first principal axes of  $\mathbf{I}$  and  $\mathbf{T}$  were strongly correlated, but the second and third were distributed more randomly in the plane perpendicular to the first. Porciani et al. (2002b) investigated the correlation between the different principal axis directions of  $\mathbf{I}$  and  $\mathbf{T}$ . They found that each principal axis of  $\mathbf{T}$  is strongly correlated with the corresponding axis of  $\mathbf{I}$ , but all at roughly the same level (to within  $\sim 15\%$ ), indicating that the strength of

the correlation is comparable between the various components, although not identical. They also find that the initial direction of  $\mathbf{L}$  (with respect to the local tidal field) for halos in their simulation is somewhat different to the direction they obtain after making  $\mathbf{I}$  and  $\mathbf{T}$  independent by randomizing the orientation of  $\mathbf{I}$ , in that the same trends are seen but they are weaker in the real simulation. This could be because of the differing strengths of  $\mathbf{I}$ – $\mathbf{T}$  correlations among different components, or it may be because higher order terms have become more important relative to the suppressed leading order term, adding larger scatter to the direction of  $\mathbf{L}$  when compared to the  $\mathbf{I}$ – $\mathbf{T}$  uncorrelated case.

So where does this leave our calculation? We expect that the larger scatter and weaker correlation between  $\mathbf{L}$  and  $\mathbf{T}$ , as compared to the predictions when there is no  $\mathbf{I}$ – $\mathbf{T}$  correlation, will cause galaxy alignments to be somewhat weaker than our prediction by some factor, making our prediction an upper limit. This is still a useful constraint, as the CNPT analysis explicitly assumes strong  $\mathbf{I}$ – $\mathbf{T}$  correlations (although see below) and so cannot be applied to the uncorrelated case to give an upper limit. Also this simple rescaling should be the only difference between our results due to the  $\mathbf{I}$ – $\mathbf{T}$  correlation, and so other differences will be due to other differences in our respective models. It is important to assess which results are robust and which are sensitive to the simplifications in both models used to calculate ellipticity. We discuss this in detail in §5. The differences seen by Porciani et al. (2002b) are not large, however, especially when compared to the effects of late-time non-linear effects also seen in their simulations, so we believe that  $\mathbf{I}$ – $\mathbf{T}$  correlations are not affecting the relevance our calculation very significantly.

### 2.3.3 Late-Time Effects on Initial Conditions

Another issue is the time dependence of a galaxy’s angular momentum. The calculation presented below is a linear theory calculation of the angular momentum acquired in the initial stages of formation. We implicitly assume that this subsequent non-linear evolution of the galaxy and its interaction with its environment do not substantially alter its angular momentum. This is almost certainly false in dense environments such as clusters of galaxies and compact groups, where the dynamical time is much shorter than the Hubble time. We expect, therefore, that our analysis will not apply to them, but rather only to more isolated galaxies. The criterion is that they should not have exchanged significant angular momentum with neighbouring galaxies/halos over a Hubble time. This is hard to quantify in practice given that galaxies form from mergers of smaller objects, so in a sense all galaxies have had many significant dynamical interactions in the past. Further, galaxies are not isolated points in the universe — they live in extended halos and it is hard to say where the halo of one galaxy stops and where the neighbouring ones start.

Sugerman et al. (2000) and Porciani et al. (2002a) indeed found that the spin direction of a dark matter halo changes with time, and that correlations between the spin direction and the initial conditions weaken significantly between the good agreement at  $z \sim 50$ , and  $z = 0$ . At  $z = 0$  there is typically a  $30$ – $40^\circ$  misalignment between the initial and  $z = 0$  spin direction. The resulting distribution is not random by any means and clearly retains some memory of the initial conditions, but the spin direction does change significantly, with most of the change happening between  $z = 3$  and  $z = 0$ . The level of the spin–spin correlation at  $z = 1$  is of order 1% at a halo separation of  $1h^{-1}\text{Mpc}$ , which is in good agreement with work by Croft & Metzler (Croft & Metzler 2000) and Heavens et al. (Heavens et al. 2000), who looked for intrinsic halo alignments in large N-body simulations.

The striking feature of the Porciani et al. (2002a) results is the decrease in the spin–spin correlation by a factor of 5 or so, as compared to the correlation at  $z = 50$ . The spin–spin correlation at  $z = 50$  is in line with TTT predictions, and it is really non-linear effects such as mergers and angular momentum exchange between halos which reduce it over time. Lee & Pen (2000) introduced a parameter ‘ $a$ ’ to account for the effects of  $\mathbf{I}$ – $\mathbf{T}$  correlations and non-linear processes on the (linear theory) correlation between spin direction and the tidal field. This results in a more random spin direction, and lower spin–spin correlations by a factor of  $a^2$ , as compared to the assumption of independent  $\mathbf{I}$  and  $\mathbf{T}$  and no non-linear effects. The Porciani et al. results indicate that it is non-linear processes acting cumulatively over time to reduce spin–spin correlations which are providing the dominant contribution to Lee & Pen’s parameter ‘ $a$ ’. This strengthens our argument that  $\mathbf{I}$ – $\mathbf{T}$  correlations do not significantly affect or invalidate our calculation, and implies that we could apply a simple correction factor to the final spin–spin correlation result to account for these non-linear effects. We note that it is not clear from the simulations if this suppression of spin–spin correlations is scale dependent or not; one might guess it is not because it seems to result from perturbing spin directions of galaxies in what is probably a fairly random manner.

Also relevant is a potentially more radical idea proposed by Vitvitska et al. (2001), who investigate the possibility that angular momentum is generated primarily by mergers and not by tidal torques. This is perhaps not unexpected in the context of hierarchical models of structure formation where galaxies form by assembly of smaller parts through mergers. In this situation, however, the TTT can still give reasonable results even though the merger details are missed. When the tidal field is smoothed over a galaxy-mass region the smaller scale fluctuations that give rise to the galaxy progenitors are erased, but the sum of all their angular momenta (which eventually gets into the galaxy through mergers) is what is calculated by the theory.

### 2.3.4 Summary of TTT

There seems to be some consensus that while tidal torque theory is not perfect, it works surprisingly well and shows that at least the outlines of what we are observing are inherent in linear theory. That TTT works at all is somewhat surprising,

considering it was first thought of in the context of top-down structure formation models wherein galaxies form via the monolithic collapse of one large concentration of matter. For our purposes, it seems that TTT is a good starting point. To extend the calculation requires including non-linear effects which will add ‘noise’ to our predictions. These non-linear effects will overwrite initial correlations to some extent, and it is not yet clear whether they just add a random component to the angular momentum or if on small scales they create their own strong alignments, or both. Indeed observations by Brown et al. (2002) indicate that galaxies have a fairly strong alignment in the local universe, probably significantly stronger than that seen between halos in simulations (at least on some scales). It is difficult to compare the strength, however, because of differing statistics calculated to measure correlation.

It seems that neglecting **I–T** correlations affects our results somewhat, but probably not very significantly, and it is not clear that there is a good analytical way of taking this into account. More significant is the dilution of spin correlations over time which is seen in simulations. This could be dealt with by simply rescaling the analytically calculated correlations. It is possible (and perhaps likely), however, that since galaxies collapse to the very centres of dark matter halos, their spin direction is much less affected by late time effects than the outer regions of halos (where most of the angular momentum is), simply because there is much less of a lever arm to torque a small compact galaxy.

### 3 CALCULATION

In this section we present our main calculation. The derivation is somewhat technical and the reader interested in only the main results can skip to §3.3. Throughout we shall perform our calculation in Fourier space and express our results in terms of angular power spectra. This allows us to take advantage of much of the theory of spin-2 fields developed for the study of polarization of e-m radiation and gravitational waves (Zaldarriaga & Seljak 1997; Kamionkowski, Kosowsky & Stebbins 1997; Hu & White 1997). In §3.3 we discuss how to convert our results to real space correlation functions to compare with earlier work.

#### 3.1 Power spectra

We begin by calculating the power spectra of the ellipticities, which are each quadratic in the angular momenta (see equation (3)). In outline, we first average our expressions for the ellipticities of a galaxy over all realisations of the inertia tensor to obtain an expression in terms only of derivatives of the gravitational potential. We then decompose the spin-2 ellipticity field into scalar (gradient or electric-type modes) and pseudo-scalar (curl or magnetic-type modes) fields in Fourier space for **k**-vectors perpendicular to the line of sight. This enables us to construct 3D power spectra for the ellipticities, which are convolutions over the density power spectrum. To proceed from here, we use the Limber approximation in Fourier space to evaluate the predicted angular power spectrum for different source distributions. It is important bear in mind that in the Limber approximation *only* modes transverse to the line of sight contribute. Evaluating correlation functions in real space is a relatively simple integral over the power spectra, so we calculate these for comparison with previous theoretical estimates and observations.

Ignoring the normalization factors for now (§3.2), we have

$$\begin{aligned}\gamma_1 &= L_x^2 - L_y^2, \\ \gamma_2 &= 2L_x L_y, \\ L_i &= n_l n_j \epsilon_{ijk} \Phi_{,kl}.\end{aligned}\tag{7}$$

As discussed above, we assume that the inertia tensor (i.e. the direction  $\hat{\mathbf{n}}$ ) is independent of the tidal field. This means we can average over orientations of the inertia tensor separately to averaging over realisations of the tidal field. When we do this, we get the expectation value for a given tidal field

$$\langle L_i L_j \rangle = \frac{1}{15} \{ \epsilon_{ikl} \epsilon_{jmn} \Phi_{,lm} \Phi_{,kn} - \Phi_{,ik} \Phi_{,jk} + \delta_{ij} \Phi_{,kl} \Phi_{,kl} \}.\tag{8}$$

This equation is the same as equation (A2) in Lee & Pen (2001), up to an overall normalisation constant. Using this, we find

$$\begin{aligned}\gamma_1 &= \frac{1}{15} \{ (2\Phi_{,zz} - \Phi_{,xx} - \Phi_{,yy})(\Phi_{,xx} - \Phi_{,yy}) + 3(\Phi_{,yz}^2 - \Phi_{,xz}^2) \}, \\ \gamma_2 &= \frac{1}{15} \{ 2(2\Phi_{,zz} - \Phi_{,xx} - \Phi_{,yy})\Phi_{,xy} - 6\Phi_{,xz}\Phi_{,yz} \},\end{aligned}\tag{9}$$

where now  $\gamma_i$  have been averaged over the distribution of inertia tensors. The projection of these ellipticities onto the plane of the sky will be a spin-2 field as in weak lensing analysis. We can construct scalar (grad or *E*-mode) and pseudo-scalar (curl or *B*-mode) functions of the ellipticities by taking derivatives. We do this in Fourier space, because the analysis is somewhat simpler and more transparent, and in the end provides a clearer physical understanding of our results. Because the ellipticity is quadratic in the gravitational potential, the Fourier transform  $\tilde{\gamma}_1(\mathbf{k}) \equiv \int d^3\mathbf{x} \gamma_1(\mathbf{x}) e^{-i\mathbf{k}\cdot\mathbf{x}}$  is a convolution over the Fourier modes of the potential. The *E*- and *B*-modes are given by (Stebbins 1996; Kamionkowski et al. 1998)

$$\begin{aligned}\epsilon(\mathbf{k})k^2 &= (k_x^2 - k_y^2)\tilde{\gamma}_1(\mathbf{k}) + 2k_x k_y \tilde{\gamma}_2(\mathbf{k}), \\ \beta(\mathbf{k})k^2 &= -2k_x k_y \tilde{\gamma}_1(\mathbf{k}) + (k_x^2 - k_y^2)\tilde{\gamma}_2(\mathbf{k}).\end{aligned}\tag{10}$$

Note that we will be working entirely in the flat sky approximation, as any correlations present will go to zero on large scales. So we obtain

$$\begin{aligned}\epsilon(\mathbf{k})k^2 &= \frac{1}{15} \int \frac{d^3\mathbf{k}'}{(2\pi)^3} \tilde{\Phi}(\mathbf{k}') \tilde{\Phi}(\mathbf{k} - \mathbf{k}') f_\epsilon(\mathbf{k}'_\perp, \mathbf{k}_\perp - \mathbf{k}'_\perp, k'_z), \\ \beta(\mathbf{k})k^2 &= \frac{1}{15} \int \frac{d^3\mathbf{k}'}{(2\pi)^3} \tilde{\Phi}(\mathbf{k}') \tilde{\Phi}(\mathbf{k} - \mathbf{k}') f_\beta(\mathbf{k}'_\perp, \mathbf{k}_\perp - \mathbf{k}'_\perp, k'_z),\end{aligned}\quad (11)$$

where  $\mathbf{k}'$  is the convolution variable, and  $f_{\epsilon,\beta}$  are functions containing all the information on the relative orientations of  $\mathbf{k}$  and  $\mathbf{k}'$  and hence the information on the derivatives of  $\Phi$ . They are given by

$$\begin{aligned}f_\epsilon(\mathbf{a}, \mathbf{b}, c) &= \frac{1}{2}(2c^2 - a^2)(b^4 + (\mathbf{a} \cdot \mathbf{b})^2 - (\mathbf{a} \times \mathbf{b})^2 + 2b^2(\mathbf{a} \cdot \mathbf{b})) \\ &\quad + \frac{1}{2}(2c^2 - b^2)(a^4 + (\mathbf{a} \cdot \mathbf{b})^2 - (\mathbf{a} \times \mathbf{b})^2 + 2a^2(\mathbf{a} \cdot \mathbf{b})) \\ &\quad + 3c^2((\mathbf{a} + \mathbf{b})^2(\mathbf{a} \cdot \mathbf{b}) + 2(\mathbf{a} \times \mathbf{b})^2), \\ f_\beta(\mathbf{a}, \mathbf{b}, c) &= (2c^2 - a^2)(b^2 + (\mathbf{a} \cdot \mathbf{b}))(\mathbf{a} \times \mathbf{b}) \\ &\quad - (2c^2 - b^2)(a^2 + (\mathbf{a} \cdot \mathbf{b}))(\mathbf{a} \times \mathbf{b}) \\ &\quad + 3c^2(a^2 - b^2)(\mathbf{a} \times \mathbf{b}).\end{aligned}\quad (12)$$

Here  $\mathbf{a}$  and  $\mathbf{b}$ , the components of  $\mathbf{k}'$  and  $(\mathbf{k} - \mathbf{k}')$  perpendicular to the line of sight, are two dimensional vectors in the plane of the sky and hence their cross product is a (pseudo)scalar quantity. Because we obtained these expressions from a convolution, they should be symmetric under the interchange of  $\mathbf{k}'$  and  $(\mathbf{k} - \mathbf{k}')$ , and this can be easily verified. It is also clear that the  $E$ -mode is a scalar and the  $B$ -mode is a pseudo-scalar.

The power spectrum is defined by

$$\langle \epsilon(\mathbf{k}) \epsilon^*(\mathbf{k}') \rangle = (2\pi)^3 \delta(\mathbf{k} - \mathbf{k}') P_{\epsilon\epsilon}(k), \quad (13)$$

and is given by

$$\begin{aligned}\langle \epsilon(\mathbf{k}_1) \epsilon^*(\mathbf{k}_2) \rangle k_1^2 k_2^2 &= \frac{1}{225} (2\pi)^3 \delta(\mathbf{k}_1 - \mathbf{k}_2) \int \frac{d^3\mathbf{k}'}{(2\pi)^3} P_\Phi(k') P_\Phi(|\mathbf{k}_1 - \mathbf{k}'|) \\ &\quad \times f_\epsilon(\mathbf{k}'_\perp, \mathbf{k}_\perp - \mathbf{k}'_\perp, k'_z) [f_\epsilon(\mathbf{k}'_\perp, \mathbf{k}_\perp - \mathbf{k}'_\perp, k'_z) + f_\epsilon(\mathbf{k}_\perp - \mathbf{k}'_\perp, \mathbf{k}'_\perp, -k'_z)],\end{aligned}\quad (14)$$

and similarly for the  $B$ -mode. Because both expressions are symmetric under the interchange of  $\mathbf{k}'$  and  $(\mathbf{k} - \mathbf{k}')$  though, the power spectrum becomes somewhat simpler:

$$\langle \epsilon(\mathbf{k}_1) \epsilon^*(\mathbf{k}_2) \rangle k_1^2 k_2^2 = \frac{1}{225} (2\pi)^3 \delta(\mathbf{k}_1 - \mathbf{k}_2) \int \frac{d^3\mathbf{k}'}{(2\pi)^3} P_\Phi(k') P_\Phi(|\mathbf{k}_1 - \mathbf{k}'|) 2f_\epsilon^2(\mathbf{k}'_\perp, (\mathbf{k}_\perp - \mathbf{k}'_\perp), k'_z). \quad (15)$$

We now need to evaluate the functions  $f_{\epsilon,\beta}$  and perform the convolution integral. Since we only consider  $\mathbf{k}$  perpendicular to the line of sight, we choose our Cartesian axes such that  $\mathbf{k} = k(1, 0, 0)$ , and we choose polar angles defined so that  $\mathbf{k}' = \alpha k(\cos\theta, \sin\theta \cos\phi, \sin\theta \sin\phi)$  with  $\alpha \equiv k/k'$ . In this coordinate system,  $|\mathbf{k} - \mathbf{k}'| = k\sqrt{1 + \alpha^2 - 2\alpha\mu}$  (where  $\mu = \cos\theta$ ) with no dependence on  $\phi$ . We find that

$$\begin{aligned}[f_\epsilon(k, \alpha, \mu, \phi)]^2 &= k^{12} \alpha^4 [(\alpha^2 - (1 + 2\alpha^2)\mu^2 + 2\alpha\mu^3 + (1 - \alpha^2 + \alpha\mu)(1 - \mu^2) \cos\phi^2)]^2 \\ [f_\beta(k, \alpha, \mu, \phi)]^2 &= k^{12} \alpha^4 (1 - \mu^2)(\alpha - \mu)^2 (1 - 2\alpha\mu)^2 \sin^2\phi.\end{aligned}\quad (16)$$

Integrating over  $d\phi/(2\pi)$  gives functions which are polynomials in  $\mu$  and  $\alpha$ . Taking a factor of  $k^{12}\alpha^4$  out of the polynomial and denoting the remainder by  $g_{\epsilon\epsilon}(\alpha, \mu)$  and  $g_{\beta\beta}(\alpha, \mu)$  we find

$$\begin{aligned}g_{\epsilon\epsilon}(\alpha, \mu) &= \frac{1}{8} ((1 + \alpha^4)(3 - 14\mu^2 + 19\mu^4) + 2\alpha(3\mu - 2\mu^3 - 17\mu^5) \\ &\quad + \alpha^2(2 - 17\mu^2 + 44\mu^4 + 19\mu^6) + 2\alpha^3(\mu + 2\mu^3 - 19\mu^5)), \\ g_{\beta\beta}(\alpha, \mu) &= \frac{1}{2} (\alpha - \mu)^2 (1 - 2\alpha\mu)^2 (1 - \mu^2).\end{aligned}\quad (17)$$

Now the power spectrum is given by

$$P_{\epsilon\epsilon}(k) = \frac{2k^8}{225} \int \frac{k^3 \alpha^2 d\alpha d\mu}{(2\pi)^2} P_\Phi(\alpha k) P_\Phi(k\sqrt{1 + \alpha^2 - 2\alpha\mu}) \alpha^4 g_{\epsilon\epsilon}(\alpha, \mu) + k_{||}\text{-terms}. \quad (18)$$

where  $k_{||}$ -terms indicates terms with line-of-sight component  $k_{||} \neq 0$  which will not contribute to our final result. The cross power spectrum  $P_{\epsilon\beta}(k)$  is identically zero as it is parity violating. We use Poisson's equation, and express the ellipticity power spectrum in dimensionless form as

$$\Delta_{\epsilon\epsilon}^2(k) = \frac{1}{225} \left( \frac{3}{2} \Omega_m H_0^2 \right)^4 \int \frac{d\alpha}{\alpha} \Delta_m^2(\alpha k) \int_{-1}^1 d\mu \frac{\Delta_m^2(k\sqrt{1+\alpha^2-2\alpha\mu})}{(1+\alpha^2-2\alpha\mu)^{7/2}} g_{\epsilon\epsilon}(\alpha, \mu) + \dots, \quad (19)$$

and similarly for the  $B$ -mode power spectrum. Here  $\Delta_m^2$  is the contribution to the mass variance per  $\log k$

$$\Delta_m^2(k) \equiv \frac{d\sigma^2}{d \log k} = \frac{k^3 P(k)}{2\pi^2}. \quad (20)$$

To proceed to the angular power spectrum we use the Limber approximation. In Fourier space the Limber approximation states that the angular power spectrum of a projection,  $\int d\chi w(\chi) S$ , of a scalar field  $S(\mathbf{x})$ , is (Kaiser 1992; White & Hu 2000)

$$\frac{\ell(2\ell+1)C_\ell}{4\pi} = \frac{\pi}{\ell} \int \chi d\chi w^2(\chi) \Delta_{SS}^2(k\chi = \ell, a), \quad (21)$$

where  $w(\chi)$  is the weight function at radial distance  $\chi$ . Before we compute our final result we need to return to the issue of the normalization constant  $C$ .

### 3.2 Normalisation

We determine  $C$  empirically by fitting the model prediction for the mean-square source ellipticity to that which is observed,

$$\begin{aligned} \bar{\epsilon}^2 &\equiv \langle \gamma_1^2 + \gamma_2^2 \rangle \\ &= C^2 \langle (L_x^2 + L_y^2)^2 \rangle. \end{aligned} \quad (22)$$

We are assuming here that all of a galaxy's ellipticity is due to its angular momentum acquired via tidal torques. It is likely that some fraction of the ellipticity is due to other effects (e.g. halo shapes as in CKB) in which case our normalisation provides an upper limit to the angular momentum correlations.

Averaging over all orientations of  $\mathbf{L}$  we find

$$\bar{\epsilon}^2 = \frac{8C^2}{15} \langle L^4 \rangle = \frac{24C^2}{15} \langle L^2 \rangle^2. \quad (23)$$

The expectation value of  $L^2$  is calculated (Catelan & Theuns 1996) to obtain

$$\bar{\epsilon}^2 = \frac{32C^2}{1125} \left( \frac{3}{2} \Omega_m H_0^2 \right)^4 \sigma^4(R), \quad (24)$$

where all the time dependent terms and the magnitude of the inertia tensor have been absorbed into the constant  $C$ . Note  $C \propto 1/\langle L^2 \rangle$  so any time dependence in  $L$  cancels out in the expressions for  $\gamma_i$ . We can therefore calculate everything according to linear theory extrapolated to the present ( $a = 1$ ). Also, the magnitude of  $L$  is irrelevant in our calculation; what is important is the ratio of  $L^2$  to the mean squared value  $\langle L^2 \rangle$ . The quantity,

$$\sigma^2(R) \equiv \int \frac{dk}{k} \Delta_m^2(k, a=1) \left( \frac{3j_1(kR)}{kR} \right)^2, \quad (25)$$

is the variance of the density field smoothed on a scale  $R$ , associated with the size of a galaxy mass region in the initial density field. We will take  $R = 1h^{-1}\text{Mpc}$ , but calculate the dependence of our results on this choice in §4.1. Finally we obtain the normalised ellipticities,

$$\begin{aligned} \gamma_1 &= \sqrt{\frac{1125}{32} \frac{\bar{\epsilon} (L_x^2 - L_y^2)}{\left( \frac{3}{2} \Omega_m H_0^2 \right)^2 \sigma^2(R)}}, \\ \gamma_2 &= \sqrt{\frac{1125}{32} \frac{\bar{\epsilon} 2L_x L_y}{\left( \frac{3}{2} \Omega_m H_0^2 \right)^2 \sigma^2(R)}}. \end{aligned} \quad (26)$$

We take  $\bar{\epsilon} = 0.4$  to present our results, as it is a good fit to the observed rms galaxy ellipticity (see CNPT).

### 3.3 Summary

We are now in a position to derive our central result. Including the normalisation factors from §3.2, we obtain the angular power spectrum

$$\frac{\ell(2\ell+1)C_\ell^{\epsilon\epsilon}}{4\pi} = \frac{5\bar{\epsilon}^2}{32\sigma^4(R)} \frac{\pi}{\ell} \int \chi d\chi w^2(\chi) \int \frac{d\alpha}{\alpha} \Delta_m^2\left(\frac{\alpha\ell}{\chi}\right) \int_{-1}^1 d\mu \frac{\Delta_m^2(\ell\sqrt{1+\alpha^2-2\alpha\mu}/\chi)}{(1+\alpha^2-2\alpha\mu)^{7/2}} g_{\epsilon\epsilon}(\alpha, \mu), \quad (27)$$

and similarly for the  $C_\ell^{\beta\beta}$  power spectrum. The cross-spectrum vanishes due to parity.

In integrating equation (27) the factor  $(1+\alpha^2-2\alpha\mu)^{-7/2}$  must be treated carefully near  $k \gg 1$  and  $k \simeq k'$ . We make an approximation in this region which is good to  $\leq 7$  per cent in the worst case (a low redshift galaxy distribution and  $\ell > 10^3$ ). The weight function depends on the number of sources per unit redshift. We take

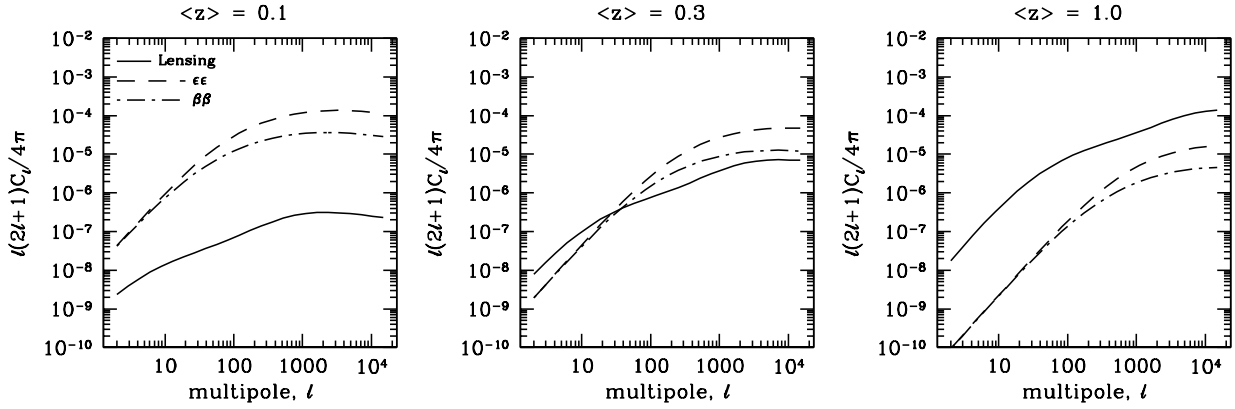


**Figure 1.** The various angular power spectra discussed in the text for our flat  $\Lambda$ CDM model. The solid line is the predicted weak lensing signal, the dashed line the “intrinsic” ellipticity  $EE$  power spectrum and the dot-dashed line the intrinsic  $BB$  power spectrum. The first panel is for a low redshift source galaxy distribution of mean redshift  $\langle z \rangle = 0.1$  using the redshift distribution described in the text. The second and third panels are for  $\langle z \rangle = 0.3$  and  $1.0$  respectively.

$$\frac{dn}{d\chi} \propto \chi^\alpha \exp \left[ - \left( \frac{\chi}{\chi_*} \right)^\beta \right], \quad (28)$$

with  $\int dn = 1$ . The case  $\alpha = 1$ ,  $\beta = 4$  approximates the source distribution of a flux limited survey, and we adjust  $\chi_*$  to obtain a desired mean source redshift (see below).

It is straightforward to go from the angular power spectrum to the correlation function. The two are related by a slight generalization of the Hankel transform as

$$\begin{aligned} \langle \gamma_1 \gamma_1 \rangle &= \int \frac{\ell d\ell}{4\pi} (C_\ell^{\epsilon\epsilon} [J_0(\ell\theta) + J_4(\ell\theta) \cos 4\phi] + C_\ell^{\beta\beta} [J_0(\ell\theta) - J_4(\ell\theta) \cos 4\phi]), \\ \langle \gamma_2 \gamma_2 \rangle &= \int \frac{\ell d\ell}{4\pi} (C_\ell^{\epsilon\epsilon} [J_0(\ell\theta) - J_4(\ell\theta) \cos 4\phi] + C_\ell^{\beta\beta} [J_0(\ell\theta) + J_4(\ell\theta) \cos 4\phi]), \end{aligned} \quad (29)$$

where the separation between the two points has polar coordinates  $(\theta, \phi)$ . For comparison with observations we also calculate the “ellipticity variance” smoothed on some angular scale  $\theta$ . This is obtained by convolving the ellipticities  $\gamma_i$  with a filter function and taking the autocorrelation of this at zero lag. For a top-hat real space circular filter of radius  $\theta$ , the variance is given by

$$\sigma^2(\theta) = \int \frac{\ell d\ell}{2\pi} (C_\ell^{\epsilon\epsilon} + C_\ell^{\beta\beta}) \left[ \frac{2J_1(\ell\theta)}{\ell\theta} \right]^2. \quad (30)$$

## 4 RESULTS

To demonstrate our results we use a flat  $\Lambda$ CDM cosmological model with parameters  $(\Omega_m, \Omega_b h^2, \Omega_\Lambda, h, n, \sigma_8) = (0.3, 0.018, 0.7, 0.67, 1.0, 0.9)$ , with the fit to the transfer function of Eisenstein & Hu (1997). Fig. 1 shows the ellipticity-ellipticity power spectra, along with the power spectrum predicted by weak lensing for three source distributions (with mean source redshifts  $\langle z_{\text{src}} \rangle = 0.1, 0.3, \text{ and } 1.0$ ).

### 4.1 Amplitude of the angular power spectra

We first discuss the overall amplitude of the intrinsic and lensing power spectra. The scales of most relevance for recent measurements of intrinsic correlations (Brown et al. 2002) and for current weak lensing surveys are from  $\ell \sim 100$  ( $\theta \sim 2^\circ$ ) to  $\ell \sim 1000$  ( $\theta \sim 10'$ ). For our low redshift galaxy sample with  $\langle z_{\text{src}} \rangle = 0.1$  the intrinsic signal dominates the weak lensing signal, while the situation is reversed for the higher redshift samples. This is one of our main results, and agrees with calculations and measurements by previous authors (CKB, CNPT, Heavens et al. 2000, Croft & Metzler 2000, Brown et al. 2000). Our result adds further support that this is the order of magnitude to expect intrinsic correlations due to correlations in the tidal field.

The result can be easily understood as the combination of two effects (these were also alluded to by Miralda-Escudé (1991) as an argument for ignoring intrinsic alignments in deep surveys). For lensing the power spectrum is proportional to the square

of the projected mass density, which increases with increasing survey depth. Intrinsic correlations, however, are located in the source plane due to galaxies physically close to each other. For deeper surveys, the probability of two galaxies close to each other on the sky being physically close to each other is much smaller than for shallow surveys. So the intrinsic correlations get ‘washed out’ by this projection effect.

This result shows that for deep weak lensing surveys with  $\langle z_{\text{src}} \rangle \sim 1.0$ , intrinsic correlations are unlikely to contribute to the signal at a significant level, as long as the redshift distribution of sources is broad. For shallower surveys, however, they are expected to be the dominant signal. This has been convincingly demonstrated by Brown et al. (2002) using the SuperCOSMOS Sky Survey. They detect a significant intrinsic correlation of the order of magnitude of our results. We compare our results with these observations in more detail in the next section.

There are two main uncertainties in the amplitude of our prediction. The first is that for very large  $\ell$ , we expect non-linear clustering of galaxies to erase the initial correlations due to interactions with neighbouring galaxies. This may randomise ellipticities altogether, or it may create new correlations with a different amplitude and scale dependence. Also, based on numerical results, the overall amplitude of the signal may be scaled down by some factor, due to the weakening of spin-spin correlations over time. Secondly, the smoothing scale in our normalisations affects our results. We use  $R = 1h^{-1}\text{Mpc}$  as the comoving scale containing on average a galaxy mass ( $10^{11}M_{\odot}$ ) at the background density. Our results scale as  $\sigma^{-4}(R)$ , so changing the smoothing scale alters things significantly. For our cosmological model, with  $\sigma_8 = 0.90$ , we find that  $\sigma(R) = 3.6, 2.8$  and  $2.0$  for  $R = 0.5, 1.0$  and  $2.0h^{-1}\text{Mpc}$  respectively. With these numbers, increasing (decreasing) our smoothing scale by a factor of two increases (decreases) our results by a factor of 3.5 (2.9).

The rms ellipticity of galaxies empirically fixes the normalisation. We choose  $\bar{e} = 0.4$  as it is unlikely to be larger than this, but it may be somewhat smaller. As stated earlier, it is also possible that only a fraction,  $f < 1$ , of the rms ellipticity is determined by the angular momentum, with the rest contributed by other processes (e.g. halo shapes). In this case our results should be multiplied by this factor of  $f$ , thus lowering the predicted power spectrum. We show all our results assuming  $f = 1$  to emphasize how large intrinsic correlations could be.

## 4.2 Power Spectrum Shape

The shape of the intrinsic power spectra is similar for all three redshift distributions, and is reflective of the underlying physics. On large scales (small  $\ell$ ) the (log) slope is 2 for both the  $EE$  and  $BB$  power spectra, consistent with shot noise ( $C_{\ell}^{ee} = C_{\ell}^{\beta\beta} = \text{constant}$ ). This is expected as there should be no intrinsic correlation between sources that are widely separated on the sky. The lensing signal falls off more slowly at large angles because it is an integral over the power spectrum whereas the intrinsic signal is an integral over the square of the power spectrum. Also lensing occurs between us and the source galaxies, whereas intrinsic correlations are at the source.

The power begins to fall significantly below the shot noise power on an angular scale corresponding roughly to the turnover in the mass power spectrum at the mean source redshift. The linear theory power spectrum changes slope at  $k \sim 0.02h \text{ Mpc}^{-1}$ , and  $k\chi \sim \ell$  at the mean redshift, so we can work out what value of  $\ell$  we expect this feature in  $\Delta_m^2(k)$  to show up. Mean redshifts of  $z = 0.1, 0.3$  and  $1.0$  correspond to distances of  $\chi = 280, 730$  and  $1650h^{-1}\text{Mpc}$  in our cosmological model. Thus we expect the roll over to occur at roughly  $\ell \sim 6, 15$  and  $35$  for the three source distributions in Fig. 1. This is indeed what we see in that the  $E$ - and  $B$ -modes start to differ from each other and to change slope for larger values of  $\ell$ .

The large  $\ell$  slope flattens off (and may even start to decrease for the low redshift population) due to the fact that the 3D matter power spectrum becomes flat at large  $k$ . We emphasize again, however, that on very small angular scales our predictions may be completely overwritten by non-linear clustering effects.

## 4.3 Ratio of $E$ - to $B$ -mode power

The  $E$ -mode intrinsic signal is enhanced over the  $B$ -mode by a factor of  $C_{\ell}^{ee}/C_{\ell}^{\beta\beta} \simeq 3.5$  on small scales ( $\ell \gg 1$ ). This goes to a constant ratio for all three galaxy redshift distributions, just shifted to smaller angular scales for deeper surveys. On very small scales the power spectrum becomes roughly constant (increases only as  $\log k$ ), so this ratio must be determined by the geometry of the problem and the tensor nature of the source. A similar result was obtained by (Hu & White 1997) in studying the polarisation induced in the CMB by tensor perturbations (gravitational waves), where they found that the ratio tended to  $C_{\ell}^{ee}/C_{\ell}^{\beta\beta} = 13/8$  in the small angle limit. Given the mathematical similarity between polarization and galaxy ellipticities, it is likely that similar geometrical considerations are producing the  $B$ -mode suppression in our model, although the suppression is stronger in our case.

An intuitive way of thinking about this  $B$ -mode suppression is that an isolated point mass can generate only  $E$ -modes. We believe that this is the reason our  $B$ -modes are suppressed on smaller scales where the density field can be increasingly described in terms of ‘objects’. As shown by Lee & Pen (2001), if the tidal field has ordered eigenvalues  $\lambda_1 \geq \lambda_2 \geq \lambda_3$  along its principal axes then (in this principal axes frame)  $L_1 \propto (\lambda_2 - \lambda_3)I_{23}$  and similarly for the other components. If  $\mathbf{I}$  and  $\mathbf{T}$  are uncorrelated we expect  $L_2$  to be largest from the ratio of the sizes of the eigenvalues. Porciani, Dekel & Hoffman (2002b) showed that in their simulations, in general  $L_1$  is smaller than the other components, so the angular momentum is largely in the plane perpendicular to the first principal axis of  $\mathbf{T}$ . This can be understood by considering a proto-galaxy forming in the vicinity of a large point mass (or equivalently a large spherically symmetric mass distribution). In the limit that the tidal field is dominated by this mass, the first principal axis of  $\mathbf{T}$  will lie in the radial direction (i.e. along the separation vector between

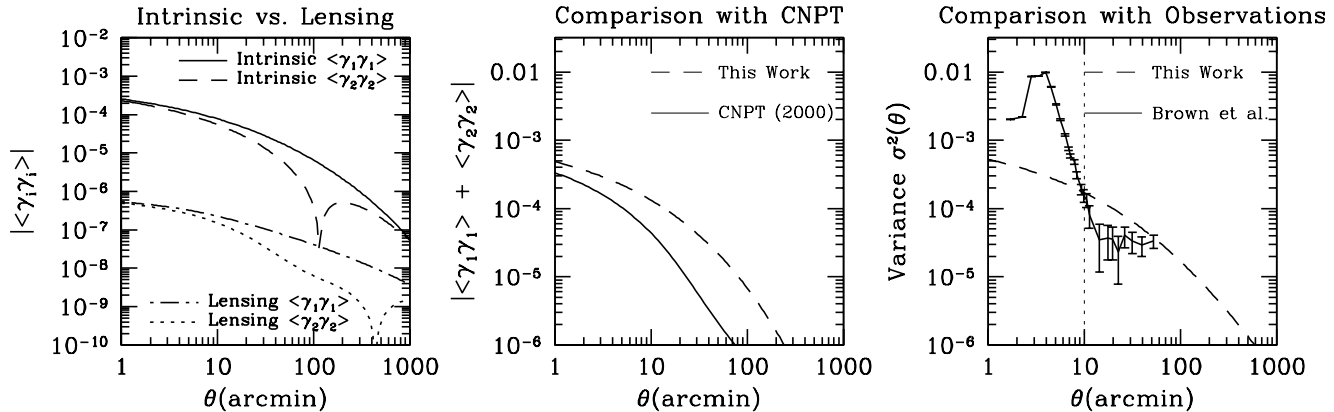


**Figure 2.** Correlation functions and comparison with other work, all for the low redshift ( $z$ ) = 0.1 source distribution. Note that different quantities are plotted on each panel, with a different y-axis scale on the first one. Left panel: Comparison of the correlation functions for intrinsic ellipticity correlations (in our model) and lensing induced correlations, as calculated from the power spectra in Fig. 1. Middle panel: Comparison with the theoretical results of CNPT. Plotted is the sum of the two correlation functions in each case. Curve is from Fig. 5 of CNPT for  $a = 0.24$ . Note the similarity of our results, although the amplitude of our result is slightly larger. Right panel: Comparison with the observations of Brown et al. (2000). Plotted is the ellipticity variance as described in the text. The vertical line at  $10'$  corresponds to a linear scale of roughly  $1h^{-1}\text{Mpc}$  at the mean source redshift, below which we do not expect our calculation to be relevant.

the proto-galaxy and the point mass), and the second and third will be in the tangential directions. The second and third eigenvalues are identical, because there is no preferred tangential direction, making  $L_1 = 0$ . Thus the angular momentum acquired due to tidal torques will be perpendicular to its separation vector from the point mass, and hence the galaxy will be oriented radially. This is a pure  $E$ -mode pattern. To see this in the context of our calculation, notice that only the radial first derivative of  $\Phi$  is non-zero, so all cross derivatives  $\Phi_{,ij}$  (with  $i \neq j$ ) vanish. These cross derivatives become cross products of  $k$ -modes in Fourier space, so inspection of equation (12) shows that the  $B$ -mode must vanish. So if the shear field is dominated by isolated point masses, then the correlations will be mostly  $E$ -modes.

That our model produces  $B$ -modes at all is due to the ellipticity components  $\gamma_i$  being quadratic in  $\mathbf{L}$  and hence in  $\Phi(\mathbf{x})$ . This can be seen in our expression for  $\beta(\mathbf{k})$  in equations (11) and (12) as a convolution over the Fourier modes of the potential. Examination of equations (11,12) shows that most of the contribution comes when  $\mathbf{k}$  and  $\mathbf{k}'$  are quite different in magnitude. We interpret this as indicating that large-scale perturbations on the small-scale potential field generate the  $B$ -modes.

One of the main ways of discriminating between weak lensing and systematic effects is that weak lensing produces only  $E$ -mode power. Shot noise has  $C_\ell^{e\epsilon} = C_\ell^{\beta\beta} = \text{constant}$ , so looking at the  $B$ -modes gives an estimate of the level of noise in the  $E$ -mode lensing signal. Our model indicates that there can be significantly larger intrinsic  $E$ -mode power than would be naively be expected from looking at the level of  $B$ -mode power. Thus the suppression of the  $B$ -modes in our model means that intrinsic correlations may be hidden in a low signal-to-noise detection of  $E$ -mode power. On the other hand, this factor of 3.5 suppression should be an upper limit to a real measurement. Adding shot noise, with  $C_\ell^{e\epsilon} = C_\ell^{\beta\beta}$ , will only reduce the  $E$ - to  $B$ - ratio. Non-linear effects adding small-scale correlations may also alter the ratio.

## 5 DISCUSSION AND COMPARISON WITH OTHER WORK

### 5.1 Correlation Functions and Comparison with CNPT and Simulations

We calculated correlation functions from the power spectra in Fig. 1 using equation (29) for the low redshift source distribution. These are plotted in the left panel of Fig. 2. In evaluating equation (29) we use  $\phi = 0$ , corresponding to the separation vector of the two galaxies being along the  $x$ -axis. Note that the  $\langle\gamma_2\gamma_2\rangle$  function goes anticorrelated for large separations, and so we plot its absolute value. The physics producing the curves is less clear than in the power spectrum analysis, but they do show the same basic features — intrinsic correlations should dominate weak lensing signal at low redshift.

Computing correlation functions allows us to compare our results with the work of CNPT who pursued a real space correlation function analysis of correlations in the orientations of galaxies. This comparison is shown in the middle panel of Fig. 2, where we are comparing with the  $a = 0.24$  curve in Fig. 5 of CNPT. <sup>†</sup> The first thing to note is that our results are broadly similar to theirs. The amplitude of our signal is slightly higher, although increasing the value of the correlation

<sup>†</sup> Note that CNPT seem to define ‘ $a$ ’ differently to Lee & Pen (2000), so that the  $a = 0.24$  they plot (and which we compare to) may not correspond exactly to the  $a = 0.24$  found by Lee & Pen in their simulations.

parameter ‘ $a$ ’ in their model can reverse this. This shows that extrapolating their model to  $a = 1$  (for the case of uncorrelated  $\mathbf{I}$  and  $\mathbf{T}$  tensors) overestimates the correlations. The reason for this is an approximation made in their calculation which assumes  $a \ll 1$ , so it was not designed to work when  $a = 1$ . It is interesting that our results only differ by  $\sim 50$  per cent at  $\theta \sim 1'$ . We would expect, because they normalise their model to take account of the suppression of spin-spin correlations seen between dark halos in numerical simulations, that their result should be significantly smaller than ours. It may be that differences in the normalisation of the underlying dark matter power spectrum, or other model differences, are decreasing the difference between our results. Overall, given the major simplifications and assumptions that go into each model, we feel it is encouraging that both models obtain similar results.

The slopes of our correlation functions are also somewhat different, with our correlation function falling off more slowly at large angular separations. We suspect that this is probably reflecting the different matter power spectra used in the calculations (CNPT used a power law whereas we use the full linear-theory power spectrum appropriate for our cosmological model), but it may also be due to differences in our models. The fact that our results are so similar adds support to the calculation of CNPT, and suggests that both their results and ours are reflecting the physics of tidal torques and not the details of our respective models.

This conclusion is further supported by recent numerical work. Heavens et al. (2000) assumed a galaxy disk will form perpendicular to the angular momentum vector of the halo it lives in and calculated spin–spin correlations from large numerical simulations. They found significant spin correlations for halos at  $z = 1$ , and less significant correlations at low redshift. At the same time, Croft & Metzler (2000) measured halo shape correlations in similar large simulations and found correlations of similar magnitude to (but slightly stronger than) the spin correlations of Heavens et al. (2000). Our results are in rough agreement with the amplitude of the signal found in these numerical simulations.

## 5.2 $E$ - and $B$ -Modes

In a second paper, Crittenden et al. (2000) calculate  $E$ - and  $B$ -mode correlation functions by constructing local estimators of the  $E$ - and  $B$ -mode contributions to the ellipticities in real space. While their method of analysis is very different to the power spectrum approach we have presented here (see Hu & White (2000) for an application of this method to simulated weak lensing data), the calculations are mathematically equivalent. We find that our results are qualitatively different from each other. For two different matter correlation functions (power laws with slopes  $-1$  and  $-3/2$ ) they find that the  $E$ - and  $B$ -mode correlation functions are the same for small separations in both cases. This is to be contrasted with the power spectra we obtain in Fig. 1, where the two are the same on large scales and differ on small scales. They also find that on large scales, for  $\xi(r) \propto r^{-1}$ , the  $E$ -modes are enhanced somewhat over  $B$ -modes, while they are identical for  $\xi(r) \propto r^{-3/2}$ . The fact that the relative contributions change depending on the power law slope of the correlation function indicates that this is the source of the difference between their results and ours. We use a power spectrum which has different large and small scale slopes to the corresponding slopes in their correlation functions, so our resulting  $E$ - and  $B$ -modes look different in the large and small angle limits. We have investigated the power spectrum dependence of the  $E/B$  ratio by considering ‘tilted’ power spectra with scalar perturbation spectral indices of  $n = (0.75, 1.25)$  as well as the canonical  $n = 1$  which we used to present our results. We find that indeed the ratio (at  $\ell = 5000$  for  $\langle z \rangle = 0.1$ ) decreases with increasing spectral index. A 25% change in  $n$  produces roughly a 12% change in the  $E/B$  ratio. The reason for this is alluded to in §4.3, where we showed that for a given value of  $\ell$ , the contributions to the  $E$ - and  $B$ -modes are from a range of different scales, and the ranges are different for the two modes. Tilting the power spectrum changes the ratios of power on different scales, and so will change the relative contributions to the  $E$ - and  $B$ -modes.

## 5.3 Comparison with Observations

In the right panel of Fig. 2 we plot the intrinsic ellipticity variance as calculated from equation (30) together with the observations of Brown et al. (2002). Observations by Pen et al. (2000) are at a similar level, but at lower statistical significance and over a smaller range of scales, so we only compare to Brown et al. here. At first sight it appears that our calculation does not fit the data very well. It is encouraging, however, that we have the right order of magnitude, and there are a number of other factors to take into account. At redshift  $z = 0.1$ , 10 arcminutes (indicated by the vertical line in the figure) projects onto a linear separation of  $\sim 1h^{-1}\text{Mpc}$ . We expect that non-linear clustering and dynamical interactions will have erased initial conditions for galaxy separations much smaller than this. Non-linear effects may produce their own alignments, and we suspect this is what is giving the large observed signal at small separations.

On larger separation scales, we have argued that our prediction should be an upper limit to correlations due to tidal torques. So the fact that we have obtained the right order of magnitude and are on the high side of the data is a good sign. The agreement of our results and the data on angular scales from  $10'$  to  $100'$  is really quite good, taking this into account. In order to conclusively test whether this observed correlation is due to correlations in the tidal field we need data that goes out to larger scales. It is important to see whether the variance stays constant as the data hint at, or whether it falls off on larger scales as the theory predicts.

## 6 CONCLUSIONS

In conclusion, we have presented a new analytic calculation of ellipticity correlations due to correlations in the tidal field galaxies form in. This correlation is probably giving the observed signal seen by (Brown et al. 2002) on scales of  $10'$  to  $100'$ . Our calculation is complementary to previous work of CNPT, who performed a similar calculation with similar input physics but different assumptions relating the physics to the observed ellipticity. The similarity of our results adds support to their validity, and indicates that they may be reflecting the physics of tidal torques rather than the detailed model assumptions.

We extend previous work in applying the Fourier space  $E$ - and  $B$ -mode power spectrum formalism to the problem (but see Crittenden et al. (2000) for an application of this decomposition in real space). We find that  $E$ -modes are enhanced by a factor of  $\simeq 3.5$  over  $B$ -modes on small scales in our model, which can be understood intuitively by noting that isolated point masses can generate only  $E$ -modes. This means intrinsic  $E$ -mode contamination of weak lensing signal can be considerably larger than that implied by looking at the  $B$ -modes. This result differs from the findings of Crittenden et al. (2000), who found that  $E$ - and  $B$ -modes have the same amplitude on small scales. This is probably mostly reflecting the different matter power spectra used in the calculations, but may also be at least partly due to differing model assumptions.

We confirm the results of previous authors in finding that intrinsic correlations are a small but possibly significant contaminant for weak lensing surveys with mean redshifts of order unity. We have shown that the contamination can be as large as 30% (in rms correlation) on degree to 10-arcmin angular scales, but this should be an upper limit according to our calculation. Thus, while at present uncertainties due to intrinsic shape correlations are at most comparable to (and probably smaller than) other observational uncertainties for deep surveys, they will become important for future precision surveys designed to put strong constraints on cosmological parameters. They will also be important for surveys in which the galaxy sample is distributed into narrow redshift bins by photometric techniques. Croft & Metzler (2000) have shown that reducing the width of the redshift distribution increases the intrinsic signal while leaving the lensing signal essentially unchanged.

Shallow surveys, on the other hand, are a very good probe of intrinsic correlations. These correlations should be investigated in more detail because they are interesting in their own right. Their existence and strength may be able put constraints on models of galaxy formation, and on the relationship between baryonic matter and dark matter halos by further comparison with numerical simulations and analytic theory.

## ACKNOWLEDGMENTS

We thank U-L. Pen, C. Metzler, R. Croft, R. Crittenden, P. Natarajan, A. Heavens and A. Refregier for useful discussions on intrinsic alignments. JM thanks R. Narayan and J. Huchra for helpful comments on an earlier draft. This work was supported in part by the Alfred P. Sloan Foundation and the National Science Foundation, through grants PHY-0096151, ACI96-19019 and AST-9803137. MK was supported at Caltech by NSF AST-0096023, NASA NAG5-8506, and DoE DE-FG03-92-ER40701. We are grateful to Lindsay King for pointing out an error in our lensing calculation.

## REFERENCES

- Abel T., Croft R., Hernquist L., 2001, [astro-ph/0111046]  
 Bacon D., Refregier A., Ellis R. S., 2000, MNRAS, 318, 625  
 Bartelmann M. & Schneider P., 1992, A&A, 259, 413  
 Bartelmann M. & Schneider P., 1999, Physics Reports, 340, 291  
 Blandford R. D., Saust A. B., Brainerd T. G., Villumsen J. V., 1991, MNRAS, 251, 600  
 Brown M. L., Taylor A. N., Hambly N. C., Dye S., 2002, MNRAS, in press, [astro-ph/0009499]  
 Cabanela J. E. & Aldering G., 1998, AJ, 116, 1094  
 Catelan P., Kamionkowski M., Blandford R.D., 2000, MNRAS, 320, 7 (CKB)  
 Catelan P. & Porciani C., 2001, MNRAS, 323, 713  
 Catelan P. & Theuns T., 1996, MNRAS, 282, 436  
 Crittenden R. G., Natarajan P., Pen U., Theuns T., 2001, ApJ, 559, 52 (CNPT)  
 Crittenden R. G., Natarajan P., Pen U., Theuns T., 2000, [astro-ph/0012336]  
 Croft R. & Metzler C., 2000, ApJ, 545, 561  
 Djorgovski S., 1987, in *Nearly Normal Galaxies*, (Springer, New York), p.227  
 Doroshkevich A. G., 1970, Afz, 6, 581  
 Eisenstein D. J., & Hu W., 1999, ApJ, 511, 5  
 Gunn J. E., 1967, ApJ, 150, 737  
 Heavens A., Refregier A., Heymans C., 2000, MNRAS, 319, 649  
 Hoyle F., 1949, in Burgers J. M., van de Hulst H. C., eds., in *Problems of Cosmical Aerodynamics* (Dayton, Ohio: Central Air Documents), p. 195  
 Hu W. & White M., 2001, ApJ, 554, 67  
 Hu W. & White M., 1997, PhRvD, 56, 596  
 Kaiser N., 1992, ApJ, 388, 272  
 Kaiser N., Wilson G., Luppino G. A., 2000, [astro-ph/0003338]  
 Kamionkowski M., Kosowsky A., Stebbins A., 1997, PhRvD, 55, 7368  
 Kamionkowski M., Babul A, Cress C., Refregier A., 1998, MNRAS, 301, 1064

- Lee J., & Pen U.-L., 2000, *ApJ*, 532, L5  
Lee J., & Pen U.-L., 2001, *ApJ*, 555, 106  
Maoli R. et al., 2001, *A&A*, 368, 766  
Mellier Y., 1999, *Ann. Rev. Astron. & Astrophys.*, 37, 127  
Miralda-Escudé J., 1991, *ApJ*, 380, 1  
Pen U.-L., Lee J., Seljak U., 2000, *ApJ*, 543, L107  
Porciani C., Dekel A., Hoffman Y., 2002a, *MNRAS*, 332, 325  
Porciani C., Dekel A., Hoffman Y., 2002b, *MNRAS*, 332, 339  
Rhodes J., Refregier A., Groth E. J., 2001, *ApJ*, 552, L85  
Stebbins A., 1996, [astro-ph/9609149]  
Sugerman B., Summers F. J., Kamionkowski M., 2000, *MNRAS*, 311, 762  
van Waerbeke L. et al., 2000, *A&A*, 358, 30  
Vitvitska M. et al, 2001, [astro-ph/0105349]  
White M. & Hu W., 2000, *ApJ*, 537, 1  
Witmann D. A. et al., 2000, *Nature*, 405, 143  
White S. D. M., 1984, *ApJ*, 286, 38  
Zaldarriaga M. & Seljak U., 1997, *PhRvD*, 55, 1830